Pergamon

Geochimica et Cosmochimica Acta, Vol. 68, No. 21, pp. 4469-4483, 2004

0016-7037/04 $30.00 + .00

doi:10.1016/j.gca.2004.04.015

Multiple sources for the origin of granites: Geochemical and Nd/Sr isotopic evidence from the Gudaoling granite and its mafic enclaves, northeast China

JIN-HUI YANG,[1,*] FU-YUAN WU,[1] SUN-LIN CHUNG,[2] SIMON A. WILDE,[3] and MEI-FEI CHU[2]

[1]Institute of Geology and Geophysics, Chinese Academy of Sciences, P.O. Box 9825, Beijing 100029, China
[2] Department of Geosciences, National Taiwan University, Taipei, Taiwan
[3]Department of Applied Geology, Curtin University of Technology, P.O. Box U1987, Perth, Western Australia 6845, Australia

(*Received January* 5, 2004; *accepted in revised form April* 7, 2004)

Abstract—Geochemical and Sr- and Nd-isotopic data have been determined for mafic to intermediate microgranular enclaves and host granitoids from the Early Cretaceous Gudaoling batholith in the Liaodong Peninsula, NE China. The rocks include monzogranite, porphyric granodiorite and quartz diorite. Monzogranites have relatively high $^{87}Rb/^{86}Sr$ ratios (0.672–0.853), low initial $^{87}Sr/^{86}Sr$ ratios (0.7052–0.7086) and $\varepsilon_{Nd}(t)$ values (−18.5 to −20.9) indicating that they were mainly derived from a newly underplated crustal source with a short crustal residence time. Quartz diorites have high initial $^{87}Sr/^{86}Sr$ ratios (0.7118–0.7120) and negative $\varepsilon_{Nd}(t)$ values (−13.2 to −18.1) coupled with high Al_2O_3 and MgO contents, indicating they were derived from enriched lithospheric mantle with contributions of radiogenic Sr from plagioclase-rich metagreywackes or meta-igneous rocks, i.e., ancient lower crust. Two groups of enclaves with igneous textures and abundant acicular apatites are distinguished: dioritic enclaves and biotite monzonitic enclaves. Dioritic enclaves have low Al_2O_3 (13.5–16.4 wt%) and high MgO (Mg# = ~72.3) concentrations, low initial $^{87}Sr/^{86}Sr$ ratios (0.7058–0.7073) and negative $\varepsilon_{Nd}(t)$ values (~−7.2), and are enriched in LILEs and LREEs and depleted in HFSEs, suggesting they were derived from an enriched lithospheric mantle source. Biotite monzonitic enclaves have Sr and Nd isotopic compositions similar to the monzogranites, indicating they were crystal cumulates of the parental magmas of these monzogranites. Granodiorites have transitional geochemistry and Nd- and Sr-isotopic compositions, intermediate between the monzogranites, quartz diorites and the enclaves.

Geochemical and Sr- and Nd-isotopic compositions rule-out simple crystal-liquid fractionation or restite unmixing as the major genetic link between enclaves and host rocks. Instead, magma mixing of mafic mantle-derived and juvenile crustal-derived magmas, coupled with crystal fractionation and assimilation of ancient lower crust, is compatible with the data. This example shows that at least some calc-alkaline granitoids are not produced by pure intracrustal melting, but formed through a complex, multi-stage hybridization process, involving mantle- and crustal-derived magmas and several concomitant magmatic processes (crystal fractionation, crustal assimilation and crustal anatexis).
Keywords—Mafic microgranular enclave, Origin for granites, Magma mixing, Sr-Nd isotopes, China

1. INTRODUCTION

Since the introduction of the terms I- and S-type granites, the source of granitic magma has become one of the most hotly debated subjects in granite petrology. Originally, I-type granites were believed to have formed by the partial melting of older igneous rocks at intracrustal levels, and that compositional variation was the result of restite composition or crystal fractionation (e.g., Chappell et al., 1987; Chappell and Stephens, 1988; Chappell and White, 1992). Although crustal recycling seems to have controlled the composition of many of these rocks, it is commonly suggested that mantle-derived magmas play a significant role in providing heat and/or mass input which contributed to the growth of continental crust (e.g., DePaolo, 1981; Holden et al., 1987; Hildreth and Moorbath, 1988; Collins, 1998; Snyder and Tait, 1998; Clynne, 1999; Millar et al., 2001). The evidence for direct contribution of mantle-derived magmas in granitoid production is often circumstantial. Intracrustal melting of older protoliths, formed by a mixture of metasedimentary and juvenile metavolcanics, or by metaigneous rocks, could also account for the observed hybrid geochemical characteristics (e.g., Clemens and Vielzeuf, 1987; Eberz et al., 1990; Turpin et al., 1990; Roberts and Clemens, 1993; Maas et al., 1997). The fact that isotopic compositions of most basic rocks related to these granitoids are heterogeneous and are rarely indicative of depleted mantle sources poses another difficulty in the assessment of this question. Two main hypotheses are envisaged for the origin of such rocks: (1) depleted mantle-derived magmas that suffered contamination by crustal rocks; or (2) enriched mantle-derived magmas.

Mafic microgranular enclaves (MMEs; see review of Didier and Barbarin, 1991) are common in intermediate to felsic granitoids and can provide significant information on the nature of the source rocks, the mechanism of production of granitic melt, the geodynamic setting of the granites, as well as evidence of interaction between continental crust and mantle. However, there are considerable discrepancies between the models proposed to explain the origin of MMEs as to whether they are restites (e.g., Chappell et al., 1987; Chen et al., 1989), or inclusions of basic magma derived from the mantle (e.g., Vernon, 1984; Bacon, 1986; Holden et al., 1987; Collins, 1998) or from the lower crust (e.g., Eberz et al., 1990; Maas et al., 1997).

* Author to whom correspondence should be addressed ((jinhui@mail.igcas.ac.cn).

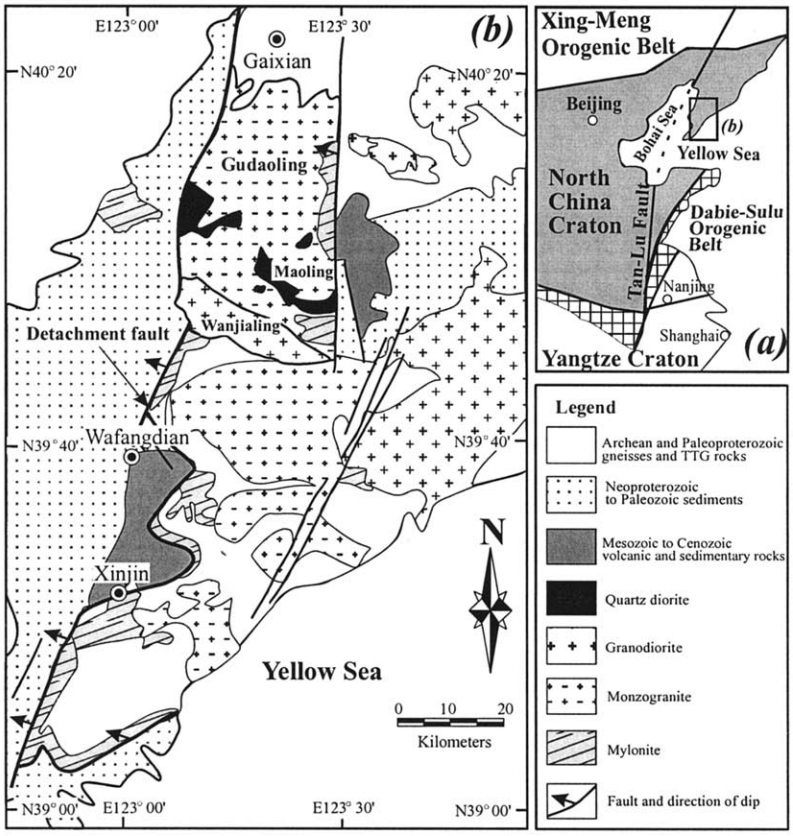

Fig. 1. Location and setting of the Gudaoling batholith in the Liaodong Peninsula, northeastern China. Inset map shows the main tectonic subdivisions of northeastern China, with study area indicated by a rectangle.

In our contribution, we present a detailed geochemical and Nd-Sr isotopic study of a suite of mafic microgranular enclaves and host granitoids from the Early Cretaceous Gudaoling batholith in the Liaodong Peninsula, northeastern China, and use these data to constrain the role of MMEs in granitic plutonism. The results suggest that the Guodaoling granitoids are a mixture of melts of enriched lithospheric mantle and both ancient and newly underplated crust. This argues against the restite model proposed by Chappell et al. (1987) and Chen et al. (1989), indicating that these granitoids were not produced by pure intracrustal melting, but require heat and melt input from mantle-derived magmas (see also Vernon, 1984; Holden et al., 1987; Collins, 1998). These results also have important implications for the lithospheric evolution and crustal architecture of the eastern segment of the North China Craton.

2. GEOLOGICAL SETTING AND GEOLOGY OF THE GUDAOLING PLUTON

2.1. Geological Setting

East China is composed of the Xing'an-Mongolia (Xing-Meng) Orogenic belt in the north, the North China Craton (NCC) in the center and the Dabie-Sulu ultrahigh-pressure orogenic belt in the south and east (Fig. 1, Wang and Mo, 1996). The Liaodong Peninsula is located in the eastern segment of the NCC and consists of Archean to Paleoproterozoic basement rocks overlain by unmetamorphosed Mesoproterozoic to Paleozoic sediments and Mesozoic to Cenozoic sedimentary and volcanic rocks (Fig. 1). Early Archean basement rocks, which range in age from 3.85 to 3.2 Ga, have been reported near Anshan, north of the Liaodong Peninsula (Fig. 1, Liu et al., 1992; Song et al., 1996). Deformed late Archean diorites, tonalites and granodiorites were emplaced at about ~2500 Ma (LBGMR, 1989). In the Paleoproterozoic, the Liaohe Group was deposited and then metamorphosed during the 1.85 Ga collisional event that is considered to mark cratonization of the NCC (Zhao et al., 2001). Subsequently, the Liaodong Peninsula was covered by a thick sequence of Meso- to Neoproterozoic and Paleozoic sediments (Wang and Mo, 1996). Paleozoic diamond-bearing kimberlite (LBGMR, 1989), Late Triassic basalt (Chen and Chen, 1997), nepheline syenite (Lin et al., 1992; Jing et al., 1995) and Cenozoic gabbro have also been found here.

In the Late Mesozoic, the Liaodong Peninsula became an important part of the circum-Pacific tectono-magmatic zone. About 20,000 km^2 of intrusive rocks have been identified, along with minor volcanic rocks (LBGMR, 1989), and these have been interpreted to result from Late Mesozoic lithospheric thinning and crustal extension in the eastern NCC (Menzies et al., 1993; Griffin et al., 1998; Wu et al., 2003; Yang et al., 2003). According to our recent work, these intrusions can be divided into two groups: 1) Jurassic (180–153 Ma) tonalite, diorite and gneissic two-mica monzogranite that have experi-

enced ductile deformation, and 2) undeformed to slightly deformed Early Cretaceous (131–120 Ma) diorite, granodiorite, monzogranite and syenogranite.

2.2. Petrography of the Gudaoling Batholith

The Cretaceous Gudaoling batholith is a syn-extensional granitoid surrounded by mylonites of the Liaonan metamorphic core complex (Fig. 1). The batholith consists mainly of monzogranite, with minor quartz diorite at Maoling and biotite granodiorite at Wanjialing (Fig. 1). The mineralogy of monzogranite is plagioclase, alkali-feldspar, quartz and biotite, with or without hornblende. Accessory minerals include apatite, zircon, titanite and Fe-Ti oxides. Granodiorites are medium- to coarse-grained with hypidiomorphic inequigranular textures due to the presence of K-feldspar megacrysts. The main minerals are quartz, plagioclase, K-feldspar, biotite and hornblende, with accessory iron oxides, apatite, zircon, and local titanite and allanite. Quartz diorites are weakly deformed, with a mineral assemblage of quartz, plagioclase and hornblende, with or without K-feldspar and biotite. Field mapping reveals the following sequence of magmatic events: (1) intrusion of quartz diorite; (2) emplacement of granodiorite; and (3) intrusion of monzogranite into the granodiorite.

MMEs have been observed locally in the Gudaoling monzogranite. They range from submillimeter up to tens of meters in size. Those recognized in the field commonly have sharp contacts with their host, are angular to oval in shape (Fig. 2) and locally occur as dike-like trails that become progressively thinner towards their termination with the host granitoid. Some mafic enclaves contain small monzogranitic enclaves (Fig. 2c), indicating that the mafic and felsic magmas were coeval. The enclaves generally have fine-grained, equigranular, hypidiomorphic textures, although ophitic textures are present in more basic varieties. Two groups of enclaves are distinguished on the basis of mineral assemblage: (a) diorite to quartz diorite and (b) monzonite enclaves. The main minerals in the dioritic enclaves are plagioclase, hornblende and quartz, with or without biotite and K-feldspar, with accessory iron oxides, apatite, zircon and local titanite and allanite. Apatite displays euhedral acicular habit. The biotite monzonite enclaves have a mineral assemblage of quartz, plagioclase, K-feldspar and biotite, with or without hornblende, different from the monzogranites with biotite contents up to 20–30%.

LA-ICP-MS U-Pb dating of zircons indicates emplacement ages for the components of the Gudaoling batholith as follows: 127 ± 4 Ma for the quartz diorite; 124 ± 2 Ma for the granodiorite; and 122 ± 2 and 118 ± 3 Ma for the biotite monzogranite. $^{40}Ar/^{39}Ar$ dating of hornblende in the dioritic enclaves gives an age of 118.4 ± 0.1 Ma, consistent with the emplacement age of the host biotite monzogranite. These results are also consistent with the field observations, where the quartz diorite is intruded and enclosed by the granodiorite and monzogranite, and the monzogranite has mingled with the mafic enclaves (Fig. 2).

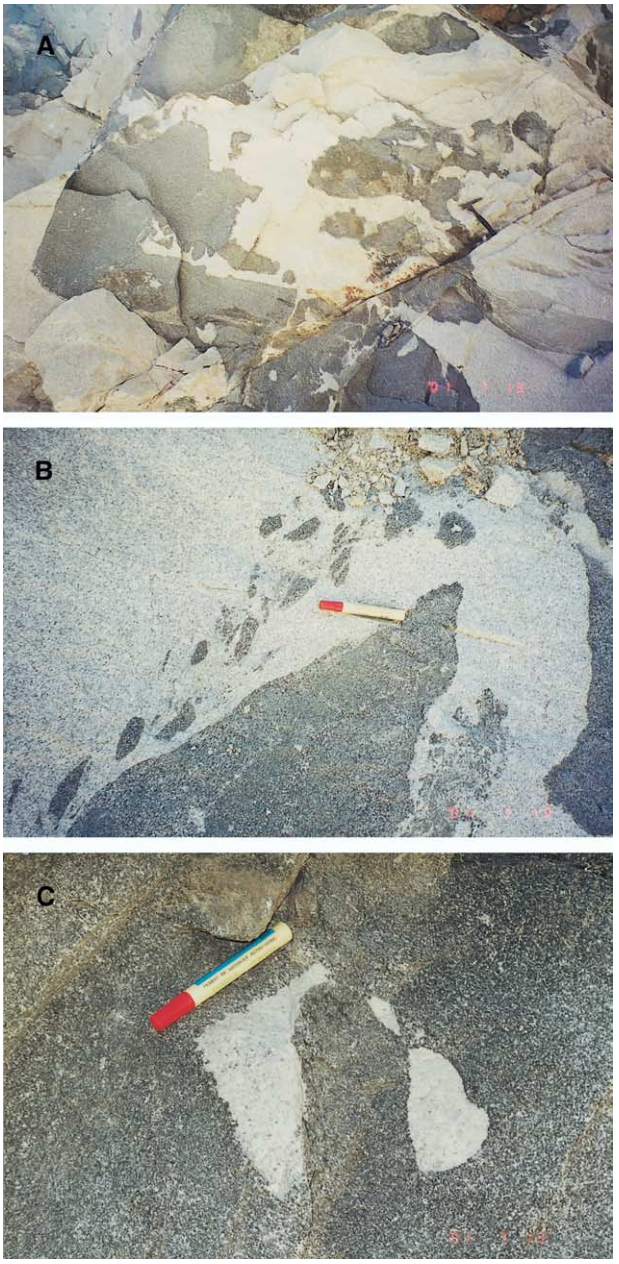

Fig. 2. Examples of (a and b) mafic microgranular enclaves (MMEs) occurring within monzogranite and (c) monzogranitic enclaves within an MME (c) in the Gudaoling batholith. Hammer is 35 cm long and pen is 14 cm long.

3. ANALYTICAL METHODS

3.1. Major and Trace Elements

After petrographic examination, 27 of the freshest samples were selected for geochemical analysis and crushed in a hardened jaw crusher and then powdered in an agate mill to < 200 mesh (75 μm). Chemical analyses were carried out at the Department of Geosciences, National Taiwan University. Major element oxides were determined by X-ray fluorescence techniques on fused glass beads using Rigaku RIX-2000 spectrometers. Trace elements were measured by inductively coupled plasma-mass spectrometry (ICP-MS, Perkin Elmer Elan-6000 spectrometer). Fused glass beads were powdered and dissolved using superpure HF and HNO_3 (10:1) mixture in screw-top Teflon beakers for 12 h at ~100 °C, followed by evaporation to dryness, and then refluxing in 7N HNO_3. After

evaporating to dryness, 2 mL HNO_3 was added, together with 10 ppb Rh as an internal standard. The internal standard was used for monitoring the signal shift during ICP-MS measurement: this showed good stability, with ~5% variation. The analytical errors are generally better than ± 5% (2σ) as shown by the statistics of duplicate analyses on five rock standards AGV-1, AGV-2, GSP-1, JB-1 and JG-1.

3.2. Nd and Sr Isotopes

Samples for isotopic analysis were dissolved in Teflon bombs after being spiked with ^{84}Sr, ^{87}Rb, ^{150}Nd and ^{147}Sm tracers before HF + HNO_3 (with a ratio of 2:1) dissolution. Rb, Sr, Sm and Nd were separated using conventional ion exchange procedures as described by Yang et al. (2004), and measured using a Finnigan MAT 262 multi-collector mass spectrometer at the Institute of Geology and Geophysics, Chinese Academy of Sciences, Beijing, China. Procedural blanks were < 100 pg for Sm and Nd and < 500 pg for Rb and Sr. $^{143}Nd/^{144}Nd$ ratios were corrected for mass fractionation by normalization to $^{146}Nd/^{144}Nd = 0.7219$ and $^{87}Sr/^{86}Sr$ ratios were normalized to $^{86}Sr/^{88}Sr = 0.1194$. Typical within-run precision (2σ) for Sr and Nd was estimated to be ±0.000015. The measured values for the La Jolla and BCR-1 Nd standards and NBS-607 Sr standard were $^{143}Nd/^{144}Nd = 0.511853 \pm 7$ ($2\sigma_n$, n = 3) and 0.512604 ± 7 ($2\sigma_n$, n = 3) and $^{87}Sr/^{86}Sr = 1.20042 \pm 2$ ($2\sigma_n$, n=12) during the period of data acquisition.

4. RESULTS

4.1. Major and Trace Elements

Granitoids of the Early Cretaceous Gudaoling batholith form part of a calc-alkaline suite that ranges in composition from quartz diorite to granodiorite and monzogranite (Fig. 3a), with an SiO_2 range from 54.2 to 72.9 wt%. The quartz diorites have higher Al_2O_3 (15.8–17.8 wt%), P_2O_5 (0.21–0.27 wt%), TiO_2 (0.70–0.89 wt%) and higher Mg# [molar 100 × MgO/(MgO + FeO_T) = 51.7–60.8] than the monzogranites (Table 1). Biotite monzogranites and granodiorites are peraluminous, with A/CNK [molar ratios $Al_2O_3/(CaO + Na_2O + K_2O)$] of 1.00–1.09 (with the exception of sample FW01-21), while quartz diorites are metaluminous with A/CNK of 0.81–0.91 (Fig. 3b). Quartz diorites have higher V, Cr, Ni, and Rb concentrations, and lower Ba concentrations and Rb/Sr ratios than either the monzogranites or the granodiorites (Table 1).

Enclaves in the Gudaoling batholith are mafic to intermediate in composition (SiO_2 51.7–60.7 wt%), corresponding to gabbro, diorite and syenodiorite in composition (Fig. 3a). The biotite monzonitic enclaves have high Al_2O_3 concentrations (>19.0 wt%) and low Mg# (27.2–32.7) and are peraluminous (A/CNK = 1.06–1.08), whereas, the dioritic enclaves have lower Al_2O_3 concentrations (<19.0 wt%) and high Mg# (44.9–72.3) and are metaluminous (A/CNK = 0.59–0.89) (Fig. 3b). The dioritic enclaves have higher V, Cr, Ni, and Rb concentrations, and lower Ba concentrations and Rb/Sr ratios than the biotite monzogranitic enclaves (Table 1).

MgO has been chosen as the abscissa for the variation diagrams, because it more effectively discriminates between these granitic to mafic rocks than SiO_2 does. Monzogranites, granodiorites and biotite monzonitic enclaves commonly define a single sequence while dioritic enclaves define another separate trend (Fig. 4). For SiO_2, TiO_2, Al_2O_3, CaO, Cr, $Na_2O + K_2O$, Rb/Sr, Sr and Sr/Y, the quartz diorites plot along a line that is the extension of the dioritic enclave data.

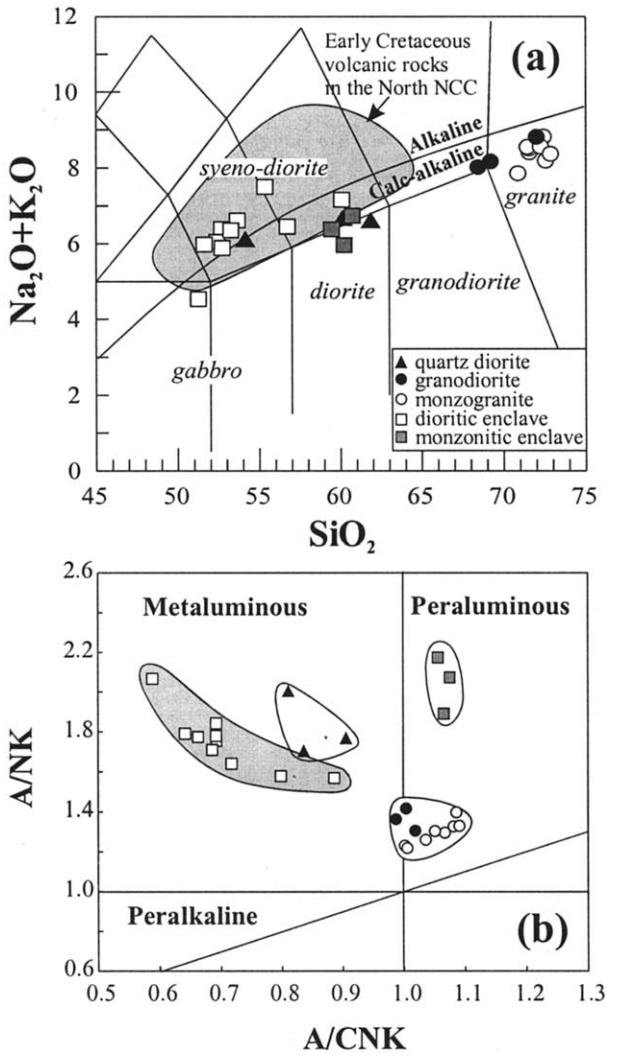

Fig. 3. Plots of (a) $Na_2O + K_2O$ vs. SiO_2 and (b) A/NK [$Al_2O_3/(Na_2O + K_2O)$] vs. A/CNK [molar ratio $Al_2O_3/(CaO + Na_2O + K_2O)$] for mafic enclaves and host granitoids from the Gudaoling batholith in the Liaodong Peninsula, northeastern China. The field of Early Cretaceous volcanic rocks in Figure 3a is from Chen and Chen (1997).

Chondrite-normalized REE patterns are shown in Figure 5. Both enclaves and host rocks have high total REE contents and are enriched in light REE. Quartz diorites have similar total REE concentrations (118–273 times chondrite) and subparallel REE patterns to monzogranites and granodiorites (Figs. 5a,b), but they have high La/Yb values and negligible negative Eu anomalies. The granodiorites and quartz diorites have higher total REE contents than the biotite monzogranites, especially for the HREEs. The $(La/Yb)_N$ ratios of quartz diorites, granodiorites, and monzogranites are high (14–76) due to HREE fractionation [$(Gd/Yb)_N = 1.8–5.9$] that suggests equilibrium partial melting with a contemporary garnet-rich residuum. Enclaves have higher ΣREE contents (Table 1 and Figs. 5c,d) than

Table 1. Major and trace element analyses of mafic microgranular enclaves and host granitoids of the Gudaoling batholith.

	FW01-350	FW01-38	FW01-18	FW01-353	FW01-21	FW01-12	JH-37	JH-38	JH-39	JH-43-2	JH-45	FW01-22	FW01-25	FW01-26
Element	Quartz diorite			Granodiorite			Monzogranite							
SiO_2	54.16	60.14	61.86	72.86	69.20	68.43	71.56	71.54	71.44	72.56	70.87	72.42	72.25	72.00
TiO_2	0.98	0.75	0.70	0.21	0.38	0.49	0.19	0.18	0.17	0.15	0.20	0.14	0.18	0.18
Al_2O_3	17.81	15.79	16.39	14.87	15.25	15.19	15.06	15.21	14.89	14.45	15.42	14.49	14.43	14.35
Fe_2O_3	7.77	5.78	5.43	1.38	2.77	3.71	1.44	1.38	1.40	0.73	1.33	1.49	2.00	1.77
MnO	0.10	0.08	0.07	0.02	0.04	0.04	0.03	0.03	0.02	0.02	0.02	0.02	0.03	0.03
MgO	4.88	4.49	2.91	0.55	0.87	0.65	0.34	0.30	0.27	0.31	0.16	0.36	0.33	0.42
CaO	7.18	5.28	4.85	1.76	2.34	2.42	1.42	1.37	1.35	1.47	1.74	1.48	1.36	1.37
Na_2O	4.14	3.74	3.86	4.12	4.14	3.61	3.96	3.94	3.95	3.92	4.47	3.93	3.86	3.95
K_2O	1.91	2.87	2.69	4.25	4.03	4.41	4.45	4.57	4.60	4.27	3.39	4.89	4.70	4.86
P_2O_5	0.27	0.21	0.21	0.09	0.14	0.17	0.07	0.06	0.06	0.05	0.05	0.07	0.07	0.07
TOT	99.70	99.58	99.54	100.38	99.56	99.53	98.51	98.58	98.16	97.91	97.64	99.61	99.51	99.62
Mg#	55.7	60.8	51.7	44.4	38.6	25.9	31.9	30.2	27.9	45.5	19.3	32.6	24.8	32.2
V	128	92	69	11.3	24	17	26	27	25	22	21	13	8.6	16
Cr	131	188	59	4.6	7.9	5.9	7.8	6.3	6.4	5.7	3.6	7.2	2.8	5.1
Ni	29	51	19	2.7	1.9	1.9	4.8	4.8	3.8	4.2	2.6	3.3	0.7	2.2
Ga	23	20	20	16	19	23	18	18	17	17	21	15	19	16
Rb	61.7	95.4	72.3	89.9	124	100	143	141	148	111	142	127	176	171
Sr	1005	673	649	551	602	516	490	487	477	447	838	555	346	404
Y	24.3	16.7	18.5	7.35	13.2	17.7	8.20	8.78	8.13	6.60	4.83	3.21	8.72	8.80
Zr	197	183	202	122	220	441	153	152	143	122	132	159	189	189
Nb	12.5	13.6	11.1	8.58	14.4	26.0	8.15	9.28	7.00	7.75	6.82	4.97	16.8	8.62
Cs	0.89	1.89	0.96	1.03	1.06	0.55	1.77	1.69	1.66	1.04	2.99	1.00	1.89	1.45
Ba	1082	952	1215	2129	1523	1987	1850	1921	1898	1449	2007	1688	1177	1531
La	43.8	54.1	31.4	76.0	61.6	95.1	42.8	34.6	33.0	32.4	28.0	34.9	64.7	54.0
Ce	93.0	92.9	61.6	140	102	169	73.7	58.9	55.2	55.1	50.2	53.2	109	85.1
Pr	11.6	10.6	7.98	12.2	10.9	19.6	7.02	5.60	5.13	5.22	5.04	5.13	11.5	8.71
Nd	47.7	37.5	32.0	39.9	36.1	70.6	23.2	18.7	17.1	17.5	17.7	15.0	37.1	27.1
Sm	7.86	5.61	5.72	4.55	5.20	11.0	3.25	2.75	2.47	2.47	2.54	1.50	5.18	3.53
Eu	2.03	1.51	1.59	1.11	1.20	2.67	0.84	0.79	0.76	0.66	0.93	0.69	0.86	0.81
Gd	6.73	5.03	4.92	4.17	4.52	9.25	2.77	2.46	2.16	2.10	2.06	1.41	4.34	3.15
Tb	0.88	0.61	0.67	0.37	0.50	1.00	0.34	0.33	0.28	0.26	0.25	0.10	0.45	0.31
Dy	4.41	3.20	3.53	1.59	2.53	4.26	1.53	1.56	1.39	1.15	1.04	0.51	1.96	1.58
Ho	0.84	0.57	0.64	0.25	0.43	0.59	0.27	0.29	0.26	0.22	0.17	0.09	0.27	0.28
Er	2.09	1.55	1.68	0.68	1.16	1.42	0.82	0.84	0.84	0.67	0.45	0.32	0.71	0.80
Tm	0.30	0.22	0.25	0.09	0.17	0.17	0.13	0.13	0.15	0.11	0.06	0.05	0.09	0.12
Yb	1.99	1.44	1.57	0.63	1.10	1.06	0.81	0.86	0.99	0.71	0.38	0.39	0.61	0.81
Lu	0.30	0.23	0.25	0.10	0.18	0.15	0.13	0.13	0.16	0.11	0.05	0.07	0.09	0.14
Hf	5.17	4.63	5.29	3.22	5.47	10.9	4.44	4.45	4.09	3.78	3.78	4.33	5.22	4.87
Ta	0.58	0.91	0.59	0.83	0.96	1.40	0.79	1.04	0.94	1.04	0.50	0.23	0.80	0.73
Pb	10	18	14	20	20	15	27	29	27	25	27	24	28	22
Th	4.8	16	5.2	19	16	12	14	12	10	9.7	5.0	9.3	19	12
U	0.90	2.55	1.02	3.21	2.08	2.05	2.03	3.77	1.34	3.35	2.16	1.26	3.63	1.51

Table 1. (Continued)

Element	JH-34	JH-35	JH-40	JH-41	JH-42	JH-44	JH-43-1	FW01-14	JH-36	JH-48	JH-46	JH-47	JH-49
	Dioritic enclave										Monzonitic enclave		
SiO_2	52.71	53.66	53.25	60.09	52.73	51.62	56.74	51.25	52.40	55.36	60.23	59.46	60.74
TiO_2	0.89	0.86	0.87	0.67	0.85	0.92	0.73	0.86	0.93	0.87	0.64	0.68	0.65
Al_2O_3	15.76	15.92	15.91	15.51	14.79	14.77	14.96	13.45	16.40	16.26	19.22	19.66	19.05
Fe_2O_3	6.68	6.27	6.50	4.44	7.02	7.03	5.78	8.21	6.67	6.76	4.70	5.41	5.10
MnO	0.11	0.10	0.11	0.07	0.12	0.15	0.11	0.13	0.10	0.10	0.07	0.08	0.08
MgO	6.70	6.21	6.64	3.99	7.50	7.21	5.67	10.72	6.30	2.75	1.14	1.01	1.02
CaO	7.56	7.63	7.70	5.26	8.12	7.66	6.43	8.97	8.11	4.38	5.13	4.83	4.28
Na_2O	3.65	3.82	3.68	3.68	3.34	3.29	3.78	2.84	4.19	3.96	4.23	4.59	4.93
K_2O	2.74	2.80	2.67	3.48	2.55	2.69	2.67	1.69	1.86	3.54	1.73	1.79	1.81
P_2O_5	0.57	0.56	0.57	0.34	0.51	0.56	0.40	0.39	0.64	0.66	0.22	0.22	0.23
TOT	97.37	97.82	97.90	97.52	97.51	95.89	97.28	99.64	97.60	94.65	97.33	97.71	97.90
Mg#	66.7	66.5	67.2	64.3	68.1	67.2	66.2	72.3	65.4	44.9	32.7	27.2	28.6
V	121	115	118	93	126	119	107	136	125	91	48	40	42
Cr	185	161	185	108	221	181	165	493	154	41	6.9	5.1	7.0
Ni	114	107	114	53	134	115	91	181	106	28	4.9	5.1	5.7
Ga	17	17	17	17	16	16	17	15	18	20	25	26	25
Rb	87.4	68.9	77.8	101	68.5	130	101	43.0	70.0	97.4	147	156	181
Sr	1085	1088	1127	852	995	916	783	814	1143	646	1307	1468	1130
Y	22.5	22.1	22.7	21.9	21.8	22.1	19.5	20.3	23.2	23.9	16.4	13.4	14.9
Zr	221	210	209	170	192	208	197	169	207	301	269	228	175
Nb	12.0	13.0	11.9	14.4	11.1	11.4	11.4	8.90	12.0	16.0	10.8	12.1	12.7
Cs	2.29	1.35	1.72	1.73	1.67	5.06	2.35	0.77	1.49	2.95	4.98	4.43	6.34
Ba	1433	1532	1488	1566	1412	1073	1321	854	713	1649	828	1053	627
La	51.1	53.6	55.5	39.7	53.7	47.9	41.7	50.5	65.8	72.0	42.8	53.6	40.3
Ce	100	103	104	76.7	99.1	91.3	80.9	94.8	117	139	86.0	104	79.7
Pr	10.9	11.0	11.1	8.42	10.5	9.87	8.77	11.8	11.9	14.9	9.72	11.2	8.78
Nd	42.6	42.1	42.6	32.7	40.3	38.7	33.9	45.0	45.3	56.6	38.7	41.8	34.1
Sm	7.11	6.87	6.96	5.71	6.69	6.39	5.69	7.54	7.31	8.59	6.51	6.02	5.51
Eu	1.99	1.95	1.92	1.48	1.86	1.74	1.60	2.08	1.88	2.11	1.63	1.56	1.15
Gd	6.17	5.93	6.12	5.02	5.76	5.55	4.97	6.51	6.39	7.22	5.10	4.81	4.53
Tb	0.88	0.85	0.86	0.77	0.83	0.81	0.72	0.81	0.91	0.96	0.70	0.60	0.62
Dy	4.38	4.18	4.28	3.96	4.10	4.08	3.62	4.09	4.46	4.47	3.15	2.59	2.86
Ho	0.82	0.79	0.81	0.75	0.77	0.76	0.68	0.73	0.84	0.82	0.56	0.45	0.49
Er	2.37	2.25	2.35	2.17	2.22	2.22	1.96	1.93	2.37	2.35	1.58	1.27	1.33
Tm	0.35	0.34	0.35	0.33	0.34	0.34	0.29	0.27	0.35	0.35	0.24	0.18	0.18
Yb	2.21	2.15	2.17	2.08	2.08	2.07	1.87	1.75	2.22	2.21	1.47	1.15	1.14
Lu	0.34	0.33	0.33	0.30	0.31	0.31	0.29	0.27	0.34	0.35	0.23	0.18	0.17
Hf	5.60	5.27	5.28	4.85	4.91	5.09	5.13	4.11	5.24	6.82	6.32	5.57	4.38
Ta	0.86	0.90	0.85	1.75	0.77	0.76	0.92	0.46	0.90	0.99	0.90	0.84	1.05
Pb	8.6	9.5	8.6	14	8.6	8.4	9.7	4.2	8.0	6.6	10	15	21
Th	8.5	9.3	9.4	9.4	9.2	8.8	10	6.3	10.3	5.4	4.3	6.1	4.4
U	2.75	3.48	2.76	3.23	2.15	3.15	6.63	1.15	3.16	0.94	1.35	1.59	1.83

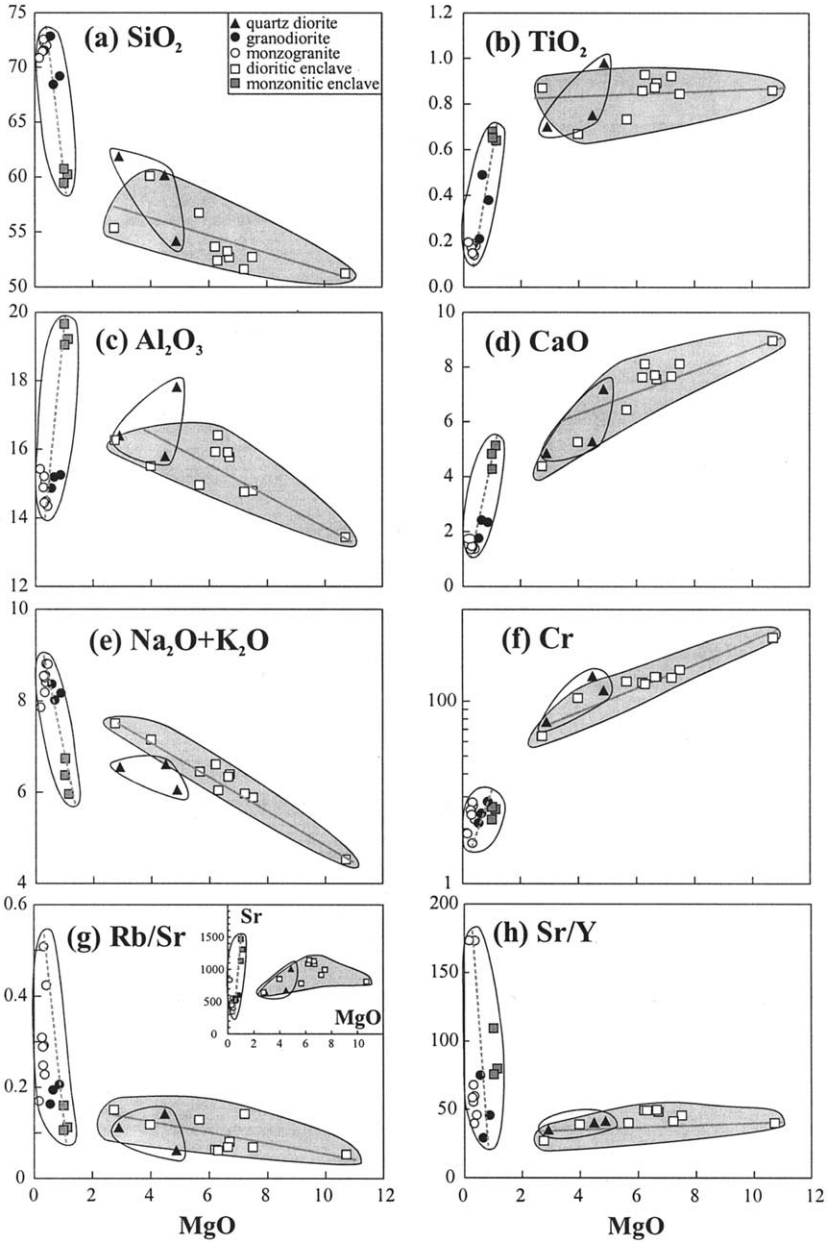

Fig. 4. Various oxide plots [(a), SiO_2,(b), TiO_2, (c), Al_2O_3, (d), CaO and (e), K_2O + Na_2O vs. MgO (all expressed in wt%)] and trace element plots [(f), Cr, (g), Rb/Sr and (h), Sr/Y] vs. MgO diagrams (expressed in ppm) for mafic enclaves and host rocks from the Gudaoling batholith in the Liaodong Peninsula, northeastern China. Solid lines indicate evolutionary trends for the mafic dioritic enclaves and dashed lines indicate trends shown by the granodiorites, monzogranites and biotite monzonitic enclaves. Quartz diorites consistently plot near the dioritic enclaves.

the monzogranites. They also have markedly higher HREE contents than the monzogranites.

In the primitive mantle (PM)-normalized trace element patterns (Fig. 6), all of these rocks are enriched in large ion lithophile elements (LILEs, such as Rb, Ba, Sr) and light rare earth elements (LREEs), and depleted in high field strength elements (HFSEs, such as Nb, Ta, P, Ti). Biotite monzonitic enclaves have similar characteristics to the host rocks, including positive Sr anomalies (Figs. 6a–c). The biotite monzonitic enclaves have relatively elevated Rb values compared to the dioritic enclaves (Figs. 6c,d).

4.2. Sr-Nd Isotope Results

Rubidium, Sr, Sm and Nd concentrations, $^{143}Nd/^{144}Nd$ and $^{87}Sr/^{86}Sr$ ratios, and T_{DM} ages for MMEs and granitoids are listed in Table 2. The initial $^{87}Sr/^{86}Sr$ ratios and $\varepsilon_{Nd}(t)$ values have been calculated at 120 Ma on the basis of zircon U-Pb and hornblende $^{40}Ar/^{39}Ar$ dating of rocks from the batholith. Depleted mantle model ages (T_{DM}) are reported using the model of DePaolo (1981). The data are shown in a plot of $\varepsilon_{Nd}(t)$ versus $(^{87}Sr/^{86}Sr)_i$ in Figure 7, and compared on that diagram with published compositional fields for Late Triassic nepheline

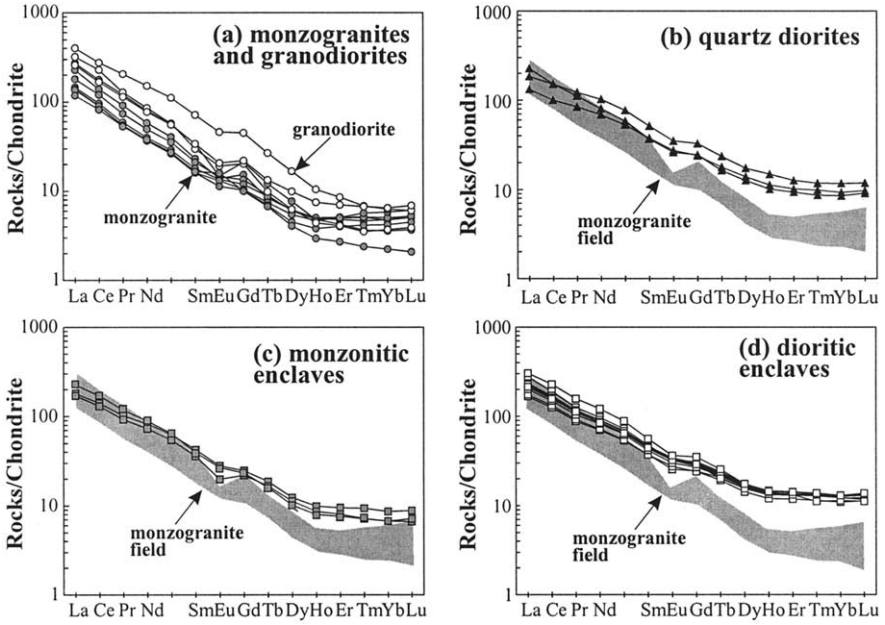

Fig. 5. Chondrite-normalized REE patterns for (a) monzogranites and granodiorites, (b) quartz diorites, (c) monzonitic enclaves, and (d) dioritic enclaves of the Gudaoling batholith. The chondrite values are from Sun and McDonough (1989).

syenites (Jing et al., 1995) and basalts (Chen and Chen, 1997) from the Liaodong Peninsula and Late Jurassic and Early Cretaceous granites and Cenozoic gabbros from the area.

The mafic enclaves and host granitoids show a large range in $(^{87}Sr/^{86}Sr)_i$ ratios (0.7055–0.7124) and $\varepsilon_{Nd}(t)$ values (−7.2 to −20.9). The monzogranites are characterized by high $^{87}Rb/^{86}Sr$ ratios and low initial $^{87}Sr/^{86}Sr$ ratios (0.70552–0.70864) and strongly negative $\varepsilon_{Nd}(t)$ values (−18.5 to −20.9). In contrast, the quartz diorites have high $(^{87}Sr/^{86}Sr)_i$ ratios (0.71185–0.71240) and relatively low $^{87}Rb/^{86}Sr$ ratios (0.1773–0.4101). The granodiorites have transitional isotopic compositions between monzogranites and quartz diorites with

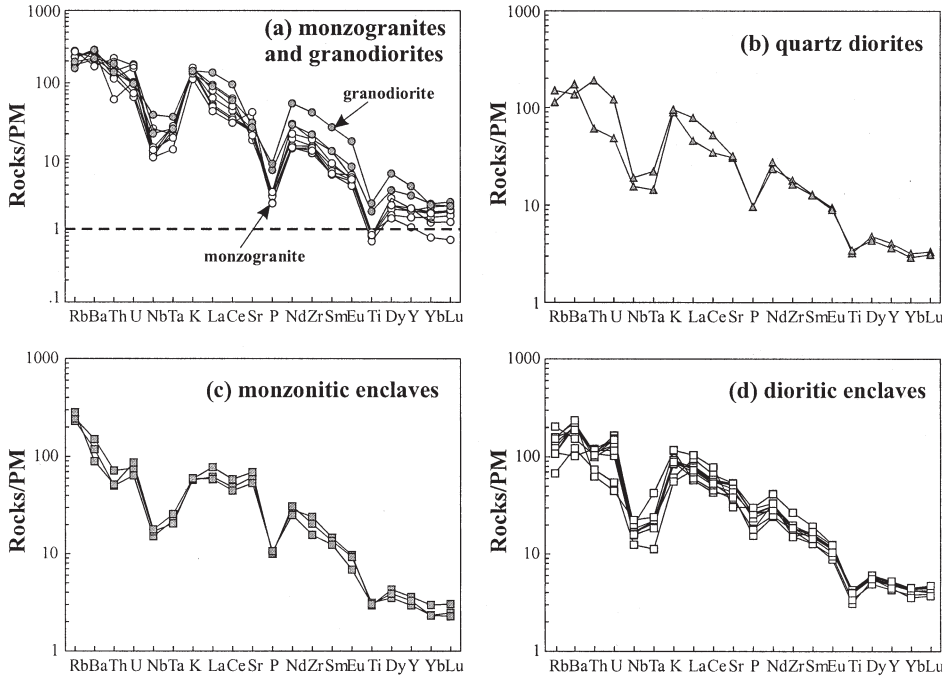

Fig. 6. Primitive mantle (PM) normalized trace element patterns, elements arranged in the order of decreasing incompatibility from left to right. (a) Monzogranites and granodiorites, (b) quartz diorites, (c) monzonitic enclaves, and (d) dioritic enclaves of the Gudaoling batholith. The PM values are from Sun and McDonough (1989).

Table 2. Rb-Sr and Sm-Nd isotopic results of mafic microgranular enclaves and host granitoids of the Gudaoling batholith.

Sample	Rock type	Rb (ppm)	Sr (ppm)	$^{87}Rb/^{86}Sr$	$^{87}Sr/^{86}Sr$	2σ	Sm (ppm)	Nd (ppm)	$^{147}Sm/^{144}Nd$	$^{143}Nd/^{144}Nd$	2σ	$(^{87}Sr/^{86}Sr)_i$[a]	$\varepsilon_{Nd}(t)$[a,b]	T_{DM} (Ma)[a,b]	$f_{Sm/Nd}$
JH-37	Monzogranite	140	486	0.8323	0.707130	11	3.10	22.7	0.0827	0.511502	10	0.70571	−20.4	1912	−0.58
JH-38	Monzogranite	145	491	0.8532	0.706979	15	2.72	18.7	0.0880	0.511494	7	0.70552	−20.6	2001	−0.55
JH-39	Monzogranite	142	481	0.8527	0.707106	11	2.34	16.7	0.0848	0.511475	8	0.70565	−20.9	1974	−0.57
JH-43-2	Monzogranite	105	448	0.6796	0.706783	13	2.22	16.0	0.0840	0.511513	11	0.70562	−20.2	1917	−0.57
FW01-22	Monzogranite	126	542	0.6716	0.709786	15	1.33	20.3	0.0396	0.511563	10	0.70864	−18.5	1387	−0.80
FW01-26	Monzogranite	195	462	1.223	0.708998	18	3.34	26.6	0.0761	0.511522	8	0.70691	−19.9	1798	−0.61
FW01-353	Granodiorite	90.5	530	0.5419	0.709305	19	4.09	31.9	0.0775	0.511647	12	0.70838	−17.4	1678	−0.61
FW01-353[c]	Granodiorite	89.9	523	0.5419	0.709323	14	3.97	32.3	0.0750	0.511603	10	0.70826	−17.8	1661	−0.63
FW01-21	Granodiorite	114	581	0.5699	0.710414	17	5.57	34.0	0.0992	0.511931	11	0.70944	−12.2	1619	−0.50
FW01-18	Qz diorite	77.7	669	0.3363	0.712969	20	4.59	25.7	0.1082	0.511638	9	0.71240	−18.1	2176	−0.45
FW01-350	Qz diorite	99.3	984	0.1773	0.712335	18	7.19	41.0	0.1059	0.511636	11	0.71203	−18.1	2133	−0.46
FW01-38	Qz diorite	92.2	651	0.4101	0.712552	17	5.19	41.28	0.0760	0.511865	19	0.71185	−13.2	1420	−0.61
JH-34	Dioritic enclave	84.0	1072	0.2266	0.706682	14	6.78	41.6	0.0987	0.512183	8	0.70630	−7.3	1280	−0.50
JH-35	Dioritic enclave	67.7	1050	0.1865	0.706579	11	7.04	44.0	0.0968	0.512189	6	0.70626	−7.2	1251	−0.51
JH-43-1	Dioritic enclave	95.2	713	0.3863	0.706451	10	5.47	32.8	0.1010	0.512149	16	0.70579	−8.0	1352	−0.49
FW01-14	Dioritic enclave	47.1	795	0.1714	0.707597	20	6.92	39.8	0.1051	0.512172	10	0.70730	−7.6	1371	−0.47
JH-48	Dioritic enclave	91.4	640	0.4132	0.705925	11	8.83	58.9	0.0906	0.511649	7	0.70522	−17.6	1853	−0.54
JH-46	Monzonitic enclave	138	1239	0.3235	0.708958	9	7.17	44.5	0.0975	0.511673	5	0.70841	−17.2	1931	−0.50
JH-47	Monzonitic enclave	147	1366	0.3119	0.708944	11	6.12	42.8	0.0864	0.511707	8	0.70841	−16.4	1724	−0.56

[a] t = 120 Ma.
[b] The $^{143}Nd/^{144}Nd$ and $^{147}Sm/^{144}Nd$ ratios of chondrite and depleted mantle at present day are 0.512638 and 0.1967, and 0.51315 and 0.222, respectively.
[c] Duplicate.

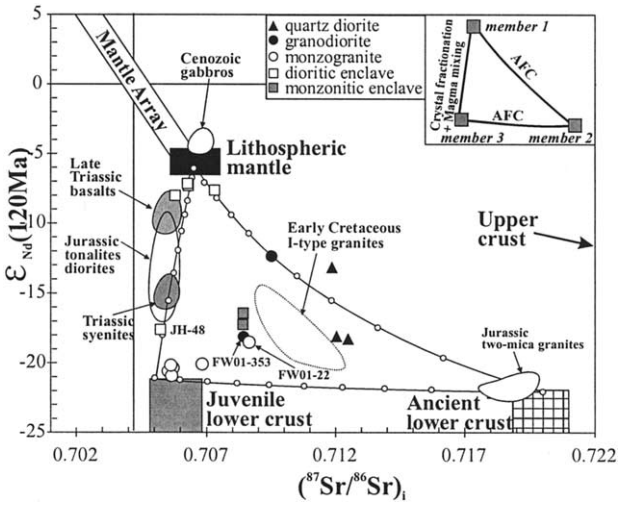

Fig. 7. $\varepsilon_{Nd}(t)$ vs. $(^{87}Sr/^{86}Sr)_i$ plot of mafic enclaves and host granitoids of the Gudoaling batholith, Liaodong Peninsula. The data for Triassic syenites and basalts are from Jing et al. (1995) and Chen and Chen (1997), respectively. The data for Jurassic granitoids (two-mica granites, diorites and tonalite), Early Cretaceous I-type granites and Cenozoic gabbros are from Wu F.-Y. (unpublished data). Superimposed on these fields are isotopic mixing curves with the dots along the three lines that link up the end members at 10% intervals. The fields were calculated as follows:

Sources	Sr (ppm)	$(^{87}Sr/^{86}Sr)_i$	Nd (ppm)	$^{143}Nd/^{144}Nd$	$\varepsilon_{Nd}(t)$
Melt from lithospheric mantle	1070	0.7065	42	0.51217	−6.0
Melt from juvenile lower crust	480	0.7050	18	0.51140	−21.0
Melt from ancient lower crust	300	0.7200	22	0.51135	−22.5

$^{87}Rb/^{86}Sr$ ratios ranging from 0.4939 to 0.5699, initial $^{87}Sr/^{86}Sr$ ratios ranging from 0.70848 to 0.70944, and $\varepsilon_{Nd}(t)$ values ranging from −12.2 to −18.2. The dioritic enclaves have a narrow range in initial $^{87}Sr/^{86}Sr$ ratios (0.70579 to 0.70730) and relatively high $\varepsilon_{Nd}(t)$ values (−7.2 to −8.0) except for one sample (JH-48) which has a low $(^{87}Sr/^{86}Sr)_i$ ratio and $\varepsilon_{Nd}(t)$ value, clearly different from those of the biotite monzonitic enclaves [$(^{87}Sr/^{86}Sr)_i$ = 0.70841 and $\varepsilon_{Nd}(t)$ = −16.4 to −17.2].

The $\varepsilon_{Nd}(t)$-$(^{87}Sr/^{86}Sr)_i$ plot (Fig. 7) highlights the following points: (1) Four of the dioritic enclaves (JH-34, −35, −43–1 and FW01-14) plot in a narrow field [$\varepsilon_{Nd}(t)$: −8.0 to −7.2; $(^{87}Sr/^{86}Sr)_i$: 0.7058 to 0.7073]; (2) four of the monzogranites (JH-37, −38, −39 and −43–2) also plot in a narrow field [$\varepsilon_{Nd}(t)$: −20.9 to −20.2; $(^{87}Sr/^{86}Sr)_i$: 0.70552 to 0.70571]; the other two samples have higher $(^{87}Sr/^{86}Sr)_i$ ratios (0.7069–0.7086) and $\varepsilon_{Nd}(t)$ values (−19.9 to −18.5); (3) quartz diorites have the highest $(^{87}Sr/^{86}Sr)_i$ ratios (0.7119–0.7124) and have negative $\varepsilon_{Nd}(t)$ values (−13.2 to −18.1); (4) the biotite monzonitic enclaves have isotopic compositions similar to the highest $(^{87}Sr/^{86}Sr)_i$ monzogranite sample (FW01-22) and lowest $(^{87}Sr/^{86}Sr)_i$ granodiorite sample (FW01-353).

5. DISCUSSION

5.1. Restite or Magma Mixing?

With the development of the restite unmixing theory (e.g., Chappell et al., 1987; Chappell and White, 1992), mafic microgranular enclaves were then incorporated in genetic models of granitoids. In this model, they are thought to represent residual material (restite) which successively unmixes from the melt during the rise of a crystal mush from its source region. A critical feature of the restite model is linear chemical variations, which are observed in many calc-alkaline plutonic suites (e.g., Chappell et al., 1987; Chappell and White, 1992; Collins, 1998). However, these features are not observed in the Gudaoling suite. In the selected oxides and trace elements versus MgO diagrams (Fig. 4), there are no converging linear trends shown that incorporate the enclaves, monzogranites and quartz diorites.

The isotopic data presented here place important constraints on the origin of microgranular enclaves. The large isotopic differences between enclaves and host rocks clearly rule out any strictly cogenetic origin. Restite derived from the source rock of the granitoids should be in isotopic equilibrium with its enclosing melt. It is therefore unlikely that the mafic microgranular enclaves from the Gudaoling batholith are restitic in origin. This view is supported by detailed microstructural observations, since the enclave textures are igneous and not metamorphic (cf. Eichelberger, 1980; Vernon, 1984).

The heterogeneous isotopic compositions of this granitoid-mafic enclave association preclude a simple, common evolution by closed-system fractionation processes. Increasing recognition that many magma chambers are open systems that may regularly be fed with more primitive magma (which can be related or unrelated to magma already in the chamber) caused a shift in the role assigned to microgranular enclaves (e.g., Vernon, 1984; Collins, 1998). Accordingly, they may also be considered to represent remnants of a mafic component added to intermediate to felsic magma chambers (e.g., Holden et al., 1987; Didier and Barbarin, 1991; Collins, 1998). In addition, the fact that they do not fit a single trend in the $\varepsilon_{Nd}(t)$ vs.

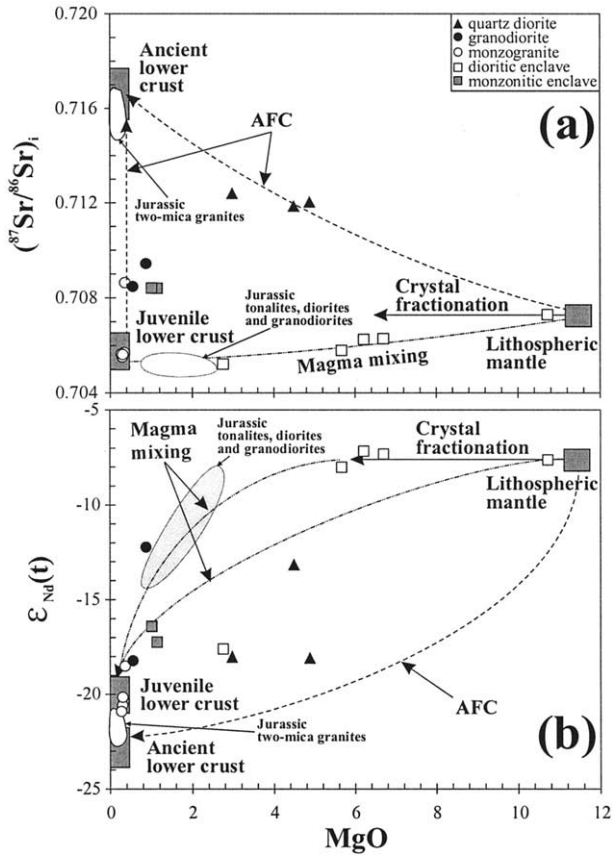

Fig. 8. Plots of (a) $(^{87}Sr/^{86}Sr)_i$ and (b) $\varepsilon_{Nd}(t)$ vs. MgO for mafic microgranular enclaves and host granitoids of the Gudaoling batholith showing crystal fractionation, crustal assimilation and magma mixing trends.

$(^{87}Sr/^{86}Sr)_i$ diagram (Fig. 7), together with the lack of evidence for converging linear geochemical trends for the enclaves, monzogranites and quartz diorites (Fig. 4) precludes a simple two-component mixing model. The enclaves may therefore represent additional components that need to be considered when interpreting the generation of their host rocks. The isotopic data (Fig. 7) may be interpreted as a result of three-component mixing among mafic [member 1: $(^{87}Sr/^{86}Sr)_i$: ~0.7058, and $\varepsilon_{Nd}(t)$: ~−7.2], intermediate or felsic [member 2: $(^{87}Sr/^{86}Sr)_i$: >0.7120, and $\varepsilon_{Nd}(t)$: <−18.2], and felsic [member 3: $(^{87}Sr/^{86}Sr)_i$: ~0.7055, and $\varepsilon_{Nd}(t)$: ~−20.9] isotopically evolved end-members, which are represented by the isotopic compositions of the dioritic enclaves, quartz diorites and monzogranites, respectively.

5.2. Mafic Magma Sources

The dioritic enclaves have increasing SiO_2, Al_2O_3, K_2O + Na_2O concentrations and decreasing CaO and Cr concentrations (Fig. 4), and constant initial $^{87}Sr/^{86}Sr$ ratios and $\varepsilon_{Nd}(t)$ values with decreasing MgO contents (Fig. 8). They have negative $\varepsilon_{Nd}(t)$ values (~−7.2) and low Nb/U (1.7–7.7) and Ce/Pb (5.4–22.4) ratios, similar to those of continental crust (Nb/U = 6.2 and Ce/Pb = 3.9; Rudnick and Fountain, 1995), but distinct from those of mid-ocean ridge and oceanic island arc basalts (MORB and OIB, Nb/U = 47 and Ce/Pb = 27, Hofmann et al., 1986). In addition, the dioritic enclaves are depleted in high field strength elements (HFSEs) with Nb and Ta anomalies and enriched in large ion lithophile elements (LILEs) and light REEs (Fig. 6d). All these features suggest that the parental magmas have been contaminated by continental crust in the source or during magma ascent, accompanied by mafic mineral fractionation.

The dioritic enclaves have high MgO (up to 10.72%), Mg# (up to 72.3), Cr (up to 493 ppm) and Ni (up to 181 ppm) at basic to intermediate silica contents, suggesting the dioritic enclaves contain a mantle component. The TiO_2 contents and $\varepsilon_{Nd}(t)$ values of samples with high Mg#, Cr and Ni contents are relatively constant with variable MgO concentrations (Figs. 4b and 8b), suggesting these samples may represent primary magma compositions that have not experienced Fe-Ti oxide fractionation and crustal assimilation during magma ascent. The low FeO and TiO_2 contents of the high-Mg# dioritic enclaves, corresponding to the component of experimental melts from depleted peridotite (Falloon et al., 1988), indicate a dominantly refractory mantle (low TiO_2, CaO/Al_2O_3, HREEs) contribution to the melt. The high-Mg# dioritic enclaves have trace element characteristics of a subduction-zone environment (Fig. 6d), for which there is no evidence in the study area. The contemporaneous formation of the Liaonan metamorphic core complex, pull-apart basins and emplacement of A-type granites with emplacement of the Gudaoling intrusion in the Liaodong Peninsula indicate an intraplate extensional environment during magma generation. Therefore, the incompatible element enrichment and subduction signatures may have been inherited from earlier subduction events, in which lithospheric mantle was metasomatized by slab-derived aqueous fluids, silicic melts or sediments (Hickey and Frey, 1982; Crawford et al., 1989; Pearce et al., 1992; Kelemen, 1995; Shimoda et al., 1998). This is similar to the formation of high-Mg boninites (e.g., Crawford et al., 1989), boninitic diorite intrusions (e.g., Kemp, 2003) and high-Mg andesites (e.g., Tatsumi and Maruyama, 1989).

Enriched isotopic and geochemical signatures are not restricted to the dioritic enclaves in the Gudaoling batholith. Similar negative $\varepsilon_{Nd}(t)$ values (−5 to −8) have been reported from Early Cretaceous mafic volcanics of the Liaodong Peninsula (Chen and Chen, 1997), indicating their derivation from similar mantle reservoirs. Furthermore, melts derived from subcontinental lithosphere beneath the Liaodong Peninsula are high-K calc-alkaline to shoshonitic in composition (Chen and Chen. 1997), which is similar to the composition of the enclaves (Fig. 3a). Therefore, we propose that the parental magmas of dioritic enclaves were derived by partial melting of enriched lithospheric mantle.

5.3. Intermediate Magma Sources

The quartz diorites are notable for having high Al_2O_3 concentrations and $(^{87}Sr/^{86}Sr)_i$ ratios but low Rb/Sr ratios, (Tables 1 and 2), suggesting involvement of melts from metagreywackes or metaigneous rocks with a near-complete breakdown of plagioclase at high pressure (Patiño Douce, 1999). However, the high MgO concentrations for both quartz diorites and granodiorites, together with their isotopic array extrapolating towards the field of dioritic enclaves (Figs. 4, 7, and 8), suggest that they resulted from the

reaction of metagreywacke or metaigneous rock with basaltic magma at high pressure. The existence of ancient metagreywackes or metaigneous rocks beneath the Liaodong Peninsula is supported by the isotopic compositions of the Jurassic gneissic granites and Archean metamorphic rocks and granites that outcrop in the area, which have high $(^{87}Sr/^{86}Sr)_i$ ratios (~0.715) and low $\varepsilon_{Nd}(t)$ values (~−22) and are interpreted to be derived from an ancient crustal source (Wan et al., 1998, 1999). Therefore, high $(^{87}Sr/^{86}Sr)_i$ metagreywackes or metaigneous rocks represent a potential crustal end-member; probably from an ancient lower crustal source.

5.4. Felsic Magma Sources

The monzogranites, granodiorites and quartz diorites of the Gudaoling batholith have Sr-Nd isotopic signatures reflecting crustal derivation, and their concave-up REE patterns with respect to MREE-HREE (Figs. 5a,b) suggest equilibrium with garnet and amphibole. Geochemical data from TTG/adakites and Na-rich granitoids from other locations (e.g., Defant and Drummond, 1990; Atherton and Petford, 1993; Martin, 1999) show similarities with the Early Cretaceous Gudaoling granitoids in terms of high Sr, low Yb and Y concentrations and high Sr/Y and La/Yb ratios (Table 1). Considering that partial melting of subducted oceanic crust or newly underplated lower crust under garnet stability conditions played an important role in the generation of TTG/adakites and Na-rich granitoids (e.g., Defant and Drummond, 1990; Atherton and Petford, 1993; Martin, 1999), these trace element characteristics can originate from partial melting of a crustal source with a high-pressure, plagioclase-poor and garnet-rich residual assemblage (Atherton and Petford, 1993; Patiño Douce, 1999).

In addition, the trace element variations can be explained by an assimilation-fractional crystallization (AFC) process involving basaltic magma (e.g., Castillo et al., 1999). The isotopic evolutionary trend of the granitoids, i.e., increasingly negative $\varepsilon_{Nd}(t)$ (−12.2 to −20.9) from intermediate quartz diorites to granodiorites and monzogranites (Table 2), is also consistent with an AFC process, combined with an increasing degree of differentiation. However, the large range in $(^{87}Sr/^{86}Sr)_i$ ratios (0.70552 to 0.71240) and the $\varepsilon_{Nd}(t)$-$(^{87}Sr/^{86}Sr)_i$ (Fig. 7) and $(^{87}Sr/^{86}Sr)_i$-MgO plots (Fig. 8) show that, except for the enriched mantle source, two distinct crustal sources, i.e., a high-$(^{87}Sr/^{86}Sr)_i$ and a low-$(^{87}Sr/^{86}Sr)_i$ source, can be distinguished.

The monzogranite samples are characterized by strongly negative $\varepsilon_{Nd}(t)$ values (~−21) combined with a relatively nonradiogenic Sr isotopic signature [$(^{87}Sr/^{86}Sr)_i \approx 0.705$] (Table 2 and Fig. 7) and show little interaction with other magmas parental to the mafic enclaves and quartz diorites. The samples with lower initial $^{87}Sr/^{86}Sr$ ratios (~0.705) have high Rb/Sr ratios (0.29–0.51), which are usually attributed to partial melting processes involving mica breakdown and/or late plagioclase fractionation. However, the absence of negative Eu anomalies in samples with lower initial $^{87}Sr/^{86}Sr$ ratios indicates the parental magmas have not experienced plagioclase fractionation. Recently, detailed studies of granitic rocks in a number of orogenic belts have identified broad positive arrays between Rb/Sr ratios of individual granite samples and the time-integrated Rb/Sr ratios of their source rocks inferred from their model neodymium ages. It means that the Rb/Sr ratios of granites can reflect the Rb/Sr ratios of their source rocks (Kemp and Hawkesworth, 2003). Therefore, the source of the monzogranites would have high Rb/Sr ratios, but low initial $^{87}Sr/^{86}Sr$ ratios, indicating it is a mica-bearing source with a short residence time. The monzogranites show elemental characteristics (e.g., high Sr, Ba and LREE, low Y and HREE, elevated La/Yb and Sr/Y ratios) that are typical of adakites, Archean TTG suites and Na-rich granitoids (Defant and Drummond, 1990; Atherton and Petford, 1993; Martin, 1999). Therefore, they have been envisaged by some workers as adakites that were derived by lower crustal melting under high pressure with a garnet-bearing residue (Zhang et al., 2001; Defant et al., 2002). We conclude that the parental magmas of the monzogranites were produced by partial melting of a juvenile basaltic lower crust. The newly underplated basaltic magmas should have a geochemistry and isotopic composition similar to that of enriched mantle, with highly negative $\varepsilon_{Nd}(t)$ values (<−15). The Sr-Nd isotopic data for the Late Triassic nepheline syenites [$(^{87}Sr/^{86}Sr)_i$ = 0.705–0.706 and $\varepsilon_{Nd}(t)$ values = −13 to −15 (Jing et al., 1995)] (Fig. 7) are similar to those of the monzogranites. It can therefore be interpreted that the source of the newly underplated magmas was similar to that of the nepheline syenites.

5.5. Genesis of the Gudaoling Batholith

Based on the magma sequence, petrography, major and trace element geochemical data and Sr and Nd isotopic compositions of mafic microgranular enclaves and host granitic rocks, a complex, multi-stage process involving magma mixing, crystal fractionation, wall-rock assimilation, and crustal anatexis of three distinct sources is proposed for the formation of the Gudaoling granitoids.

The monzogranites with low initial $^{87}Sr/^{86}Sr$ ratios and highly negative $\varepsilon_{Nd}(t)$ values were mainly derived by partial melting of juvenile basaltic lower crust coupled with crystal fractionation and little or no involvement of other components, such as enriched lithospheric mantle or ancient lower crust. However, the samples with higher initial $^{87}Sr/^{86}Sr$ ratios (up to 0.70864) and $\varepsilon_{Nd}(t)$ values up to −18.5, most likely originated from partial melting of 80–90% juvenile lower crust, followed by crystal fractionation, but mixed with mantle-derived magmas and assimilated ancient crustal materials (Fig. 7).

The granodiorites and quartz diorites were the result of interaction between a mantle-derived magma and ancient lower crustal materials, with involvement of juvenile lower crustally derived magma. Sr-Nd isotopic calculations indicate that 60–70% mantle, 5–10% juvenile lower crust and 20–30% ancient lower crustal material is compatible with the data.

The dioritic enclaves with $\varepsilon_{Nd}(t)$ values of ~−7.2 were derived from an enriched lithospheric mantle with fractional crystallization and little involvement of crustal materials. The biotite monzonitic enclaves have similar isotopic compositions to the monzogranite (e.g., FW01-22), indicating that they were mainly produced by fractional crystallization of magmas parental to the monzogranites.

5.6. Implications for Crustal Architecture

There is a progressive change in composition of plutonic rocks in the Liaodong Peninsula with time (Fig. 9), reflecting a

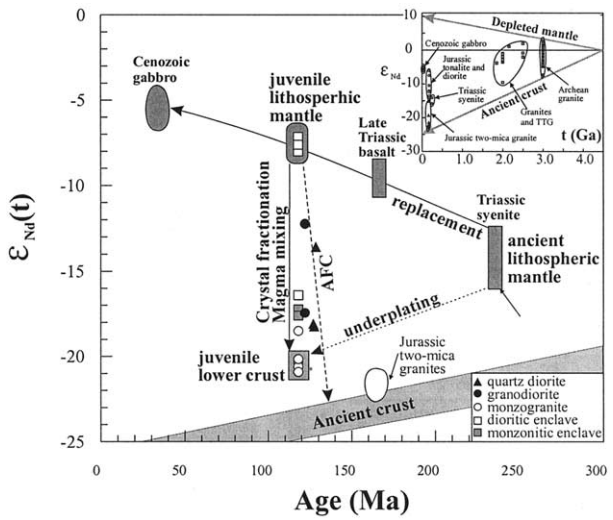

Fig. 9. Plot of $\varepsilon_{Nd}(t)$ vs. Age (Ma) for mafic enclaves and host granitoids from the Gudaoling batholith, compared with Jurassic granites, shows the lithospheric evolution of the Liaodong Peninsula. Fields of Triassic syenites and basalts, Jurassic granitoids, and Cenozoic gabbros as defined in Figure 7. The data for Precambrian TTG suites and granites are from Song et al. (1996) and Wan et al. (1998, 1999). The inset map showing the evolution of depleted mantle and ancient crust with time.

change from continental crust/ancient lithospheric mantle sources in the Late Triassic to juvenile continental crust/lithospheric mantle sources in the Early Cretaceous. This may be explained by the replacement of ancient lithospheric mantle by juvenile lithospheric mantle during the Late Jurassic to Early Cretaceous, which is consistent with the fact that lithospheric mantle beneath the eastern North China Craton has been thinned considerably since the Phanerozoic, as evidenced by geophysical and geochemical data (Menzies et al., 1993; Griffin et al., 1998; Wu et al., 2003; Yang et al., 2003).

We provide the following synthesis of major events in the region during this time period:

(i) Metagreywackes and/or metaigneous rocks represent a common lower crustal component of the Liaodong Peninsula before underplating by mantle-derived magma from melting of an ancient lithospheric source prior to the formation of the Gudaoling granitoids. The underplate contributed substantially to crustal thickness and these magmas had low $(^{87}Sr/^{86}Sr)_i$ and $\varepsilon_{Nd}(t)$ values similar to the Late Triassic nepheline syenites.

(ii) Ancient lithospheric mantle was replaced by younger, less refractory lithospheric mantle in the eastern part of the North China Craton, as evidenced by high surface heat flow, uplift and basin development, slow seismic wave velocities in the upper mantle, and changes in the Nd isotopic compositions of mantle-derived rocks and in the character of mantle xenoliths sampled by Paleozoic to Cenozoic magmas (Griffin et al., 1998; Wu et al., 2003; Yang et al., 2003).

(iii) Basaltic magmas derived from juvenile lithospheric mantle underwent fractional crystallization during uprise into the continental crust and induced anatexis of the lower crust. Both mantle-derived and anatectic magmas mixed together, and coupled with AFC processes, gave rise to magmas ranging from quartz diorite to biotite monzonite in composition. The dioritic enclaves represent the tangible remains of these mantle-derived magmas, whereas the biotite monzonitic enclaves are products of crystal fractionation of the magmas which were parental to the monzogranites.

6. CONCLUDING REMARKS

Mafic microgranular enclaves and host granitoids of the Gudoaling batholith in the Liaodong Peninsula of NE China provide direct evidence of the involvement of mantle-derived magmas in granitoid genesis. Geochemical and Sr and Nd isotopic compositions support multiple sources for their origin.

Basic magmas were emplaced penecontemporaneously with granitoids and were contaminated during their ascent by crustal components. Although it is difficult to deduce precise estimates for the isotopic signature of the basaltic component, the available data suggest that a magma with high MgO, negative $\varepsilon_{Nd}(t)$ and high $(^{87}Sr/^{86}Sr)_i$, i.e., partial melts of enriched refractory lithospheric mantle and its evolved products, were involved in the hybridization process. Monzogranites with low $(^{87}Sr/^{86}Sr)_i$ ratios and negative $\varepsilon_{Nd}(t)$ values are interpreted as representatives of a crustal end-member generated during this process. These were derived by fractionation or partial melting of sources with a short time-integrated Rb/Sr ratio, such as newly underplated crust. Another crustal end-member, ancient lower crust, is identified in the quartz diorites and biotite monzonitic enclaves that were the result of interaction between metagreywackes and/or metaigneous rocks and ascending basalt magma.

The Gudaoling plutonic association thus illustrates that hybridization of mantle-derived magmas and crustal components is a complex, multi-stage process involving several different mechanisms (magma mixing, crystal fractionation, and wall-rock assimilation) which all operated together during the Late Mesozoic in the Liaodong Peninsula of NE China.

Acknowledgments—J. H. Yang benefited from a 1-yr stay in the Department of Geosciences, National Taiwan University. We thank Profs. Guang-Sheng Qiao and Ren-Hu Zhang and Drs. Zhu-Yin Chu and Chao-Feng Li for helping with Sr and Nd isotopic analyses. Grahame Oliver commented on an earlier draft and we thank Charles R. Bacon and P. T. Leat for their constructive reviews and Martin Menzies (AE), Frank A. Podosek (EE), and Linda Trower (EM) for handling the manuscript. This study was supported by grants NSFC-40325006, 40132020 and 40133020, the "Funds for Hundred Outstanding Talents Plan," and KZCX1-07.

Associate editor: M. Menzies

REFERENCES

Atherton M. P. and Petford N. (1993) Generation of sodium-rich magmas from newly underplated basaltic crust. *Nature* **362,** 144–146.

Bacon C. R. (1986) Magmatic inclusions in silicic and intermediate volcanic rocks. *J. Geophys. Res*. **91,** 6091–6112.

Castillo P. R., Janney P. E., and Solidum R. (1999) Petrology and grechemistry of Camiguin Island, southern Philippines: Insight into the source of adakite and other lavas in a complex arc tectonic setting. *Contrib. Minerl. Petrol*. **134,** 33–51.

Chappell B. W. and Stephens W. E. (1988) The origin of infracrustal (I-type) granite magmas. *Trans. R. Soc. Edinburgh Earth Sci*. **79,** 71–86.

Chappell B. W., White A. J. R., and Wyborn D. (1987) The importance of residual source material (restite) in granite petrogenesis. *J. Petrol*. **28,** 1111–1138.

Chen Y. D., Price R. C., White A. J. R., and Chappell B. W. (1989) Inclusions in three S-type granites from southeastern Australia. *J. Petrol*. **30,** 1181–1218.

Chappell B. W. and White A. J. R. (1992) I- and S-type granites in the Lachlan Fold Belt. *Trans. R. Soc. Edinburgh Earth Sci*. **83,** 1–26.

Chen Y. X. and Chen W. J. (1997) *Mesozoic Volcanic Rocks in West Liaoning and Adjacent Areas*. Seismological Publishing House, Beijing.

Clemens J. D. and Vielzeuf D. (1987) Constraints on melting and magma production in the crust. *Earth Planet. Sci. Lett*. **86,** 287–306.

Clynne M. A. (1999) A complex magma mixing origin of rock erupted in 1915, Lassen Peak, California. *J. Petrol.* **40,** 105–132.

Collins W. J. (1998) Evaluation of petrogenetic models for Lachlan Fold Belt granitoids: Implications for crustal architecture and tectonic models. *Austr. J. Earth Sci*. **45,** 483–500.

Crawford A. J., Falloon T. J. and Green D. H. (1989) Classification, petrogenesis and tectonic setting of boninites. In *Boninites and Related Rocks* (ed. A. J. Crawford), pp. 2–44. Unwin Hyman.

Defant M. J. and Drummond M. S. (1990) Derivation of some modern arc magmas by melting of young subducted lithosphere. *Nature* **347,** 662–665.

Defant M. J., Xu J. F., Kepezhinskas P., Wang Q., Zhang Q., and Xiao L. (2002) Adakites: Some variations on a theme. *Acta Petrol. Sinica* **18,** 129–142.

DePaolo D. J. (1981) Neodymium isotopes in the Colorado Front Range and crust-mantle evolution in the Proterozoic. *Nature* **291,** 193–196.

Didier J. and Barbarin B. (1991) *Enclaves and Granite Petrology, Developments in Petrology.* Elsevier Science.

Eberz G. W., Nicholls I. A., Maas R., McCulloch M. T., and Whiteford D. J. (1990) The Nd- and Sr-isotopic composition of microgranitoid enclaves and their host rocks from the Swifts Creek Pluton, southeast Australia. *Chem. Geol*. **85,** 119–134.

Eichelberger J. C. (1980) Vesiculation of mafic magma during replenishment of silicic magma reservoirs. *Nature* **288,** 446–450.

Falloon T. J., Green D. H., Hatton C. J., and Harris K. L. (1988) Anhydrous partial melting of a fertile and depleted peridotite from 2 to 30 kba and application to basalt petrogenesis. *J. Petrol*. **29,** 1257–1282.

Griffin W. L., Zhang A., O'Reilly S. Y., Ryan C. G. (1998) Phanerozoic evolution of the lithosphere beneath the Sino-Korean Craton. In *Mantle Dynamics and Plate Interaction in East Asia* (eds. M. F. J. Flower, S. L. Chung, C. H. Lo and T. Y. Lee), 107–126. Geodynamics Series 27.

Hickey R. and Frey F. A. (1982) Geochemical characteristics of boninite series volcanics: Implications for their source. *Geochim. Cosmochim. Acta* **49,** 1797–1811.

Hildreth W. and Moorbath S. (1988) Crustal contributions to arc magmatism in the Andes of central Chile. *Contrib. Mineral. Petrol*. **98,** 455–489.

Hofmann A., Jochum K., Seufert M., and White M. (1986) Nb and Pb in oceanic basalts: New constraints on mantle evolution. *Earth Planet. Sci. Lett*. **33,** 33–45.

Holden P., Halliday A. N., and Stepens W. E. (1987) Neodymium and strontium isotope content of microdiorite enclaves points to mantle input to granitoid production. *Nature* **330,** 53–56.

Jing Y. Z., Guo Y. J., and Ding C. X. (1995) Geochronology and origin of Saima alkaline rocks in Liaoning Province. *Liaoning Geol.* **4,** 258–271.

Kelemen P. B. (1995) Genesis of high Mg# andesites and the continental crust. *Contrib. Mineral. Petrol*. **120,** 1–19.

Kemp A. I. S. (2003) Plutonic boninite-like rocks in an anatectic setting: Tectonic implications for the Delamerian orogen in southeastern Australia. *Geology* **31,** 371–374.

Kemp A. I. S. and Hawkesworth C. J. (2003) Granitic perspectives on the generation and secular evolution of the continental crust. In *Treatise on Geochemistry,* Vol. 3, *The Crust* (ed. R. L. Rudnick), pp. 349–410. Elsevier Pergamon.

LBGMR (Liaoning Bureau of Geology and Mineral Resources) (1989) *Regional Geology of Liaoning Province* (in Chinese with English abstract). Geological Publishing House, Beijing.

Lin J. Q., Tan D. J., Chi X. G., Bi L. J., Xie C. F., and Xu W. L. (1992) *Mesozoic Granites in Jiao-Liao Peninsula* (in Chinese with English abstract). Science Press, Beijing.

Liu D. Y., Nutman A. P., Compston W., Wu J. S., and Shen Q. H. (1992) Remmants of ≥3800 Ma crust in the Chinese part of the Sino-Korean Craton. *Geology* **20,** 339–342.

Maas R., Nicholls I. A., and Legg C. (1997) Igneous and metamorphic encalves in the S-type Deddick Granodiorite, Lachlan Fold Belt, SE Australia: Petrographic, geochemical and Nd-Sr isotopic evidence for crustal melting and magma mixing. *J. Petrol*. **38,** 815–841.

Martin H. (1999) The adakitic magmas: Modern analoge of Archean granitoids. *Lithos* **46,** 411–429.

Menzies M. A., Fan W. M., and Zhang M. (1993) Palaeozoic and Cenozoic lithoprobe and the loss of >120 km of Archean lithosphere, Sino-Korean craton, China. In *Magmatic Processes and Plate Tectonics* (eds. H. M. Prichard, T. Alabaster, N. B. W. Harris and C. R. Neary), pp. 71–81. Spec. Publ. 76. Geol. Soc. Lond.

Millar I. L., Willan R. C. R., Wareham C. D., and Boyce A. J. (2001) The role of crustal and mantle sources in the genesis of granitoids of the Antarctic Peninsula and adjacent crustal rock. *J. Geol. Soc. Lond*. **158,** 855–867.

Patiño Douce A. E. (1999) What do experiments tell us about the relative contribution of crust and mantle to the origin of granitic magmas? In *Understanding Granites: Integrating New and Classical Techniques* (eds. A. Catro, C. Fernández, and J. L. Vignersse), pp. 55–76. Spec. Publ. 168. Geol. Soc. Lond.

Pearce J. A., van der Laan S. R., Arculus R. J., Murton B. J., Ishii T., Peate D. W., and Parkinson I. J. (1992) Boninite and harzburgite from Leg 125 (Bonin-Mariana forearc): A case study of magma genesis during the initial stages of subduction. In *Proceedings of the Ocean Drilling Program 94* (eds. P. Freyre and J. A. Pearce), pp. 304–316. Ocean Drilling Program.

Roberts M. P. and Clemens J. (1993) Origin of high-potassium, calc-alkaline, I-type granitoids. *Geology* **21,** 825–828.

Rudnick R. L. and Fountain D. M. (1995) Nature and composition of the continental crust: A lower crustal perspective. *Rev. Geophys*. **33,** 267–309.

Shimoda G., Tatsumi Y., Nohda S., Ishizaka K., and Jahn B. M. (1998) Setouchi high-Mg andesites revisited: Geochemical evidence for melting of subducted sediments. *Earth Planet. Sci. Lett*. **160,** 479–492.

Snyder D. and Tait S. (1998) The imprint of basalt on the geochemistry of silicic magmas. *Earth Planet. Sci. Lett*. **160,** 433–445.

Song B., Nutman A. P., Liu D. Y., and Wu J. S. (1996) 3800–2500 Ma crustal evolution in the Anshan area of Liaoning Province, northeastern China. *Precam. Res*. **78,** 79–94.

Sun S. S. and McDonough W. F. (1989) Chemical and isotopic systematics of oceanic basalts: Implications for mantle composition and processes. In *Magmatism in the Ocean Basins* (eds. A. D. Saunders and M. J. Norry), pp. 313–345. Spec. Publ. 42. Geol. Soc.

Tatsumi Y. and Maruyama S. (1989) Boninites and high-Mg andesites: Tectonics and petrogenesis. In *Boninites* (ed. A. J. Crawford), pp. 50–71. Unwin Hyman, London.

Turpin L., Cuney M., Friedrich H., Bouchez J. L., and Aubertin M. (1990) Meta-igneous origin of Hercynian peraluminous granites in NW French Massif Central: Implications for crustal history reconstruction. *Contrib. Mineral. Petrol*. **104,** 163–172.

Vernon R. H. (1984) Microgranitoid enclaves: Globules of hybrid magma quenched in a plutonic environment. *Nature* **304,** 438–439.

Wan Y. S., Liu D. Y., Wu J. S., Zhang Z. Q., and Song B. (1998) The origin of Mesoarchean granitic rocks from Anshan-Benxi area: Constraints of Geochemistry and Nd isotope. *Acta Petrol. Sinica* **14,** 278–288.

Wan Y. S., Song B., Wu J. S., Liu D. Y., and Zhang Z. Q. (1999) Geochemical and Nd and Sr isotopic compositions of 3.8 Ga trondhjemitic rocks from the Anshan area and their significance. *Acta Geol. Sinica* **73,** 25–36.

Wang H. Z. and Mo X. X. (1996) An outline of the tectonic evolution of China. *Episodes* **18,** 6–16.

Wu F. Y., Walker R. J., Ren X. W., Sun D. Y., and Zhou X. H. (2003) Osmium isotopic constraints on the age of lithospheric mantle beneath northeastern China. *Chem. Geol*. **196,** 107–129.

Yang J. H., Chung S. L., Zhai M. G., Zhou X. H. (2004) Geochemical and Sr-Nd-Pb isotopic compositions of mafic dikes from the Jiaodong Peninsula, China: Evidence for vein-plus-peridotite melting in the lithospheric mantle. *Lithos* **73,** 145–160.

Yang J. H., Wu F. Y., Wilde S. A. (2003) A review of the geodynamic setting of large-scale Late Mesozoic gold mineralization in the North China Craton: An association with lithospheric thinning. *Ore Geol. Rev*. **23,** 125–152.

Zhang Q., Qian Q., Wang E., and Wang Y. (2001) Existence of East China plateau in mid-late Yanshan period: Implication from adakites. *Sci. Geol. Sinica* **36,** 248–255.

Zhao G. C., Wilde S. A., Cawood P. A., and Sun M. (2001) Archean blocks and their boundaries in the North China Craton: Lithological, geochemical, structural and P-T path constraints and tectonic evolution. *Precam. Res*. **107,** 45–73.